Carrier mobility versus carrier density in Al$_x$Ga$_{1-x}$N/GaN quantum wells

J.-L. Farvacque[1] and Z. Bougrioua[2]

[1]*Laboratoire de Structure et Propriétés de l'Etat Solide, CNRS ESA 8008, Université des Sciences et Technologies de Lille, 59655 Villeneuve d'Ascq Cedex, France*

[2]*CHREA-CNRS, rue Bernard Gregory, 06560 Valbonne, France*

Experimental measurements show that, in Al$_x$Ga$_{1-x}$N/GaN triangular quantum wells, the free-carrier mobility experiences a strong decrease with increasing carrier density. A theoretical analysis of the various scattering mechanisms that can explain such a behavior is presented. It shows that, even though phonon and carrier-carrier scattering mechanisms naturally lead to a mobility decrease versus carrier density, they are by themselves not able to justify the whole set of experimental data. Instead, we propose to attribute an extrinsic origin to the scattering associated with the progressive appearance of strain relaxation defects and give explicit expressions for the collision time associated with interface roughness and interface charge spatial fluctuations ("electrical" roughness) which may result from the existence of cracks in Al$_x$Ga$_{1-x}$N, thickness inhomogeneity, misfit dislocations, and alloy disorder.

PACS number(s): 72.10.Fk, 72.80.Ey

I. INTRODUCTION

Heterostructures of the wurtzite nitride family offer quite an unique situation since their (0001) interfaces are expected to bear a surface charge σ_0, resulting from the difference between the spontaneous polarization appearing in such ionic materials.[1] Moreover, this charge may be increased because of a strong piezoelectric response taking place in the strained Al$_x$Ga$_{1-x}$N cap layer.[2-6] For given setups, this charge creates an attractive potential and therefore a quantum well whose filling by free carriers results from the electronic dielectric response of the whole system (Fig. 1). The (screening) free electrons come either from the ionization of free Al$_x$Ga$_{1-x}$N surface states or from bulk states. It could be shown experimentally that one does not need any intentional doping of the cap layers for obtaining large free-carrier densities contrarily to the case of quantum wells of the GaAs family. In Al$_x$Ga$_{1-x}$N/GaN quantum wells, the spontaneous interface charge plus the piezoelectric charge is so large that one can obtain free-carrier densities n_S reaching values much larger than 10^{13} cm^{-2} while, in the case of quantum wells of the GaAs family, they are only limited to values of the order of 10^{11-12} cm^{-2}. This particular situation has enhanced the interest of the device industry since a larger density of free carriers and a lack of scattering by remote ionized impurities should lead, in principle, to good conductivities and therefore to good device performances. For obtaining increasing free-carrier densities in the quantum well, it is necessary to use increasing x compositions of the Al$_x$Ga$_{1-x}$N alloy and/or to use increasing values of Al$_x$Ga$_{1-x}$N layer thickness. These requirements are a hint showing that most of the free carriers originate from the ionization of the surface or bulk states of the Al$_x$Ga$_{1-x}$N cap layer, since increasing the Al$_x$Ga$_{1-x}$N layer thickness pushes more and more these states above the Fermi level. However, doing so, experimental results clearly indicate that the carrier mobility also severely decreases with the Al$_x$Ga$_{1-x}$N cap layer thickness as well as with the x composition of the Al$_x$Ga$_{1-x}$N alloy.

To illustrate this, we are considering the case of a series of

several tens Al$_x$Ga$_{1-x}$N-GaN HEMT-like structures that we grew on c-plane sapphire substrates, in a close-coupled showerhead MOVPE reactor, using ammonia, TMGa, and TMAl as precursors. The epitaxy of both the GaN semi-insulating templates and the Al$_x$Ga$_{1-x}$N cap layer was carried out at low pressure (100 Torr). Other growth conditions are given in Ref. 10. For this study we consider structures with x varying between 15% and 45% and Al$_x$Ga$_{1-x}$N thickness vary between 11 and 54 nm. Room-temperature resistivity–Hall-electrical measurements have been carried to measure the two-dimensional (2D) carrier density and mobility. Figure 2 depicts the evolution of the mobility as a function of the carrier density. It clearly shows that the mobility decreases then quenches with increasing values of the 2D carrier density. The solid line is the polynomial tendency
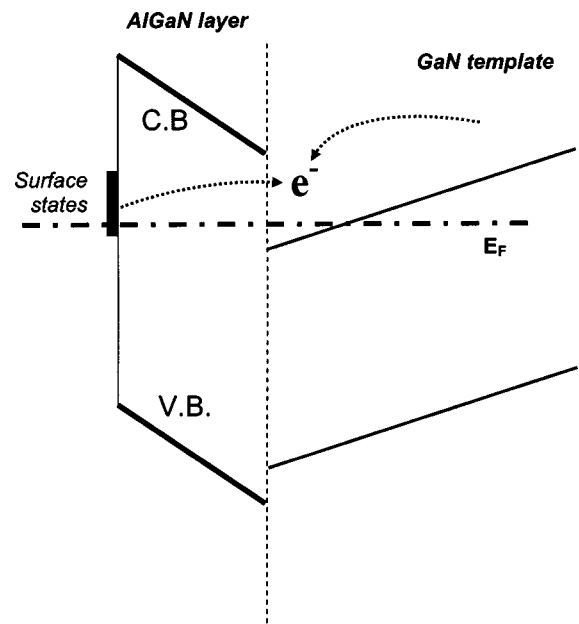
FIG. 1. Schematic representation of an Al$_x$Ga$_{1-x}$N/GaN triangular potential.
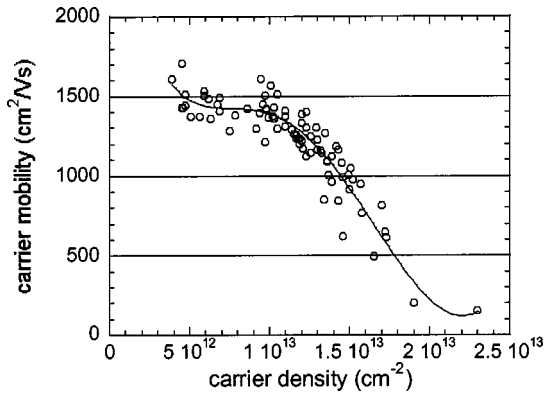
FIG. 2. Room-temperature mobility vs carrier density. Points obtained on various $Al_xGa_{1-x}N/GaN$ quantum wells grown by LP-MOCVD. The solid curve is the tendency curve (mean polynomial representative curve).

curve representing the series of experimental points, hereafter named the "empirical tendency curve."

In this paper, we present a theoretical analysis of all the scattering mechanisms that can explain such a severe decrease of the mobility versus carrier density. More particularly, we show that the unavoidable (intrinsic) scattering mechanisms associated with phonons are enhanced in two ways and justify a strong but natural decrease of the mobility with an increasing carrier density. Indeed, increasing the carrier density (i) leads, in triangular potentials, to a stronger confinement of the trapped carriers: thus a larger and larger number of phonons are involved in the scattering process, a consequence of the Heisenberg inequalities, and (ii) pushes the Fermi level at values which become larger than the optical phonon energy, allowing more and more phonon *emission* processes. Then we also consider the so-called carrier-carrier scattering as an unavoidable mechanism and conclude that, even though these scattering mechanisms theoretically lead to a first explanation of the carrier mobility decrease versus carrier density, their effects are far from explaining the severe quench experimentally observed. In a second part, we then show that this mobility decrease also results from the fact that a thicker and thicker $Al_xGa_{1-x}N$ cap layer contains more and more elastic energy, which may induce strain relaxation mechanisms (appearance of dislocations, alloy disordering, surface cracks, etc.) and therefore create new material related (extrinsic) scattering mechanisms.

For the low-field transport calculations, we have used the numerical solution of the linearized Boltzmann equation described in the first paper of this series where multisubband screening was included.[7] In the particular 2D case, the various collision times strongly depend on the actual shape of the envelope functions describing the electronic confinement in the quantum well. Thus the actual wave functions of the quantum well have been numerically determined prior to any transport calculation.

II. QUANTUM WELL ENERGY STATES

A. Numerical method

Usually, for the sake of simplicity in transport calculations, the wave functions needed for the evaluation of the various matrix elements are chosen under the form of trial analytical functions[8–10] which, in practice, only allow the description of the first subband and prevent one from considering exchange and correlation potentials. However, various self-consistent numerical approaches including Coulomb, exchange, and correlation potentials have been established in the past decades in order to obtain a true description of the energy states and their corresponding wave functions as, for instance, in Refs. 11–13. In the present work, in order to simulate the quantum well mobility and to check the effect of the carrier confinement on the various scattering mechanisms, we have determined numerically the energy states and their associated wave functions, adapting methods usually used in *ab initio* calculations to the establishment and the resolution of the envelop function equation. The Coulomb interaction and the exchange and correlation contributions[14–16] as well as the BenDaniel-Duke kinetic energy operator[17] accounting for the spatial dependence of the effective mass were introduced in the Kohn-Sham-like envelope equation. Our numerical method is based on the following assumption: since the quantum well states are localized, it is assumed that their corresponding wave functions vanish at the extremities of a segment of length L in which the quantum well potential is embedded. Thus the wave functions may be expressed as a Fourier series of planes waves that are naturally defined by the segment length L. In this plane-wave basis, the envelop function Kohn-Sham equation transforms into a matrix where the Coulomb as well as the exchange and correlation potentials are automatically calculated using the fast Fourier transform technique. The Kohn-Sham Hamiltonian matrix eigenelements are then numerically solved using an iterative procedure and their eigenvalues allow one, finally, to calculate the full quantum well energy $E_T(L)$, which turns out to be a function of the parameter L. This last value L is chosen in order to minimize E_T. This variational procedure, already used in Refs. 18 and 19 allows us to get precise numerical results with a relatively low number of planes waves (~ 50 in the present 1D localized case).

B. Energy states and wave functions in $Al_xGa_{1-x}N/GaN$ quantum wells

The numerical method described above is valid for any shape of quantum well binding potentials. In the particular case of the $Al_xGa_{1-x}N/GaN$ quantum well, it is supposed that the quantum well arises because of an intrinsic positive charge σ, issuing from the spontaneous polarization and from the piezoelectric response of the strained $Al_xGa_{1-x}N$ cap layer. This charge is localized at the interface and creates an attractive potential given by

$$W_{QW}(z) = \frac{2\pi\sigma}{\varepsilon_L}|z|. \qquad (2.1)$$

Associated with the $Al_xGa_{1-x}N/GaN$ band offset, such a bare potential creates an attractive triangular quantum well schematically shown in Fig. 1. We may suppose that the electronic density n_s contained in the well is equal to σ, leading to a globally neutral quantum well (QW). Situations
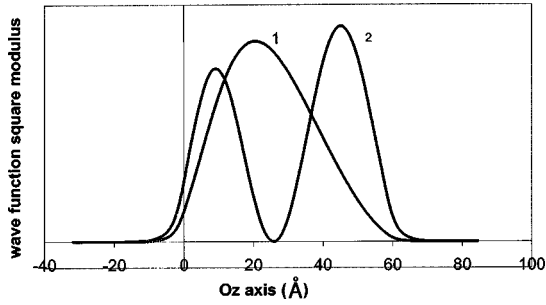
FIG. 3. Wave function square modulus of the two first energy states calculated for an $Al_xGa_{1-x}N/GaN$ quantum well with $x=0.3$ and assuming that the interface charge σ is equal to the electronic density n_s. The conduction band offset is taken equal to 75% of the band gap difference.

where $n_s < \sigma$ may, however, also be considered. As an example, Fig. 3 shows the square modulus of the two first bound wave functions in the case of a neutral QW, assuming an Al composition of 30%.

In any cases, numerical results indicate that (i) for low carrier densities ($n_s < 5 \times 10^{12}$ cm^{-2}), more than one subband are significantly occupied by electrons, justifying the multisubband formalism for the low-field transport calculation, multisubband screening effects included, (ii) an increasing carrier density leads to a stronger confinement of the electronic density which is pushed towards the interface, and (iii) the Fermi level is strongly pushed upward to large energy values and overcome 90 meV above the first energy ground state as soon as the carrier density exceeds $\sim 8 \times 10^{12}$ cm^{-2}. Note that this particular value corresponds to the optical phonon energy.

III. INTRINSIC SCATTERING MECHANISMS

Even in perfect materials, there exist two intrinsic unavoidable scattering mechanisms: (i) the existence of the electron-phonon interaction, and (ii) in the current material system, the quantum well electronic filling may reach so large carrier densities without any intentional doping, such that the carrier-carrier interaction is no more negligible. In the following, we recall the various scattering potentials associated with phonons and give explicitly an expression of their screened matrix elements. Then we have used the Episov-Levinson formula for carrier-carrier scattering.

A. Phonon scattering

1. Formalism

We suppose that the whole electron phonon system corresponds to the Hamiltonian

$$H = H_e + H_{ph} + W_{e,ph}, \qquad (3.1)$$

where $W_{e,ph}$ is a coupling operator between both electron and phonon systems. The eigenstates of H_e and H_{ph} are, respectively, $|k\rangle$ and $|N_\kappa, \kappa\rangle$ where N_κ is the number of phonons in the κ state. If we consider the coupling term $W_{e,ph}$ of Eq. (3.1) as a perturbation, then we may build the

approximate eigenstates of H as the direct product of electronic states and phonon states:

$$|n,k,N_\kappa,\kappa\rangle = |n,k\rangle |N_\kappa, \kappa\rangle. \qquad (3.2)$$

With such states, the matrix element for an electronic transition is given by

$$V_{kk'}(\kappa) = \langle n,k|\langle N_\kappa, \kappa|W_{e,ph}|N'_\kappa, \kappa\rangle|n',k'\rangle. \qquad (3.3)$$

For any type of scattering mechanisms (acoustic deformation potential, acoustic piezoelectric potential, or polar optical phonons), the various coupling operators $W_{e,ph}$ for each κ phonon momentum may be written as follows:

$$W_{e,ph,\kappa}(\vec{r}) = A(\kappa)\{a_\kappa e^{i\vec{\kappa}\cdot\vec{r}} + a_\kappa^\dagger e^{-i\vec{\kappa}\cdot\vec{r}}\}, \qquad (3.4)$$

where the well-known functions $A(\kappa)$ may be found, for instance, in Ref. 20 and where a and $a^\dagger$ are the annihilation and creation operators such that

$$\langle N_\kappa + 1|a^\dagger|N_\kappa\rangle = \sqrt{\frac{\hbar(N_\kappa+1)}{2\rho\omega_\kappa V}},$$

$$\langle N_\kappa - 1|a|N_\kappa\rangle = \sqrt{\frac{\hbar N_\kappa}{2\rho\omega_\kappa V}}. \qquad (3.5)$$

The quantity N_κ is given by Bose statistics. ρ is the material density, and V is the crystal volume. ω_κ is the phonon angular frequency. We introduce the notation $\vec{\kappa} = (\vec{q}, q_z)$ where q_z is the phonon momentum component perpendicular to the quantum well. Since absorption $(-)$ and emission $(+)$ processes are independent, considering Eq. (3.5) and using electronic wave functions of the form

$$\varphi_{j,k}(r) = \frac{1}{\sqrt{S}} e^{i\vec{k}\cdot\vec{\rho}} Z_{j,k}(z),$$

where $k = (k_x, k_y)$ and $\rho = (x,y)$ are two-dimensional vectors and where Z is the envelop function, their unscreened matrix elements are given by

$$M_{n,m}^{ext,\pm}(k,k',q_z)$$

$$= A(\vec{q}, q_z)\delta_{k', k\mp q}\sqrt{\frac{\hbar(N_\kappa + 1/2 \pm 1/2)}{2\rho\omega_\kappa V}} I_{n,m}^\pm(q_z), \qquad (3.6)$$

where we have defined

$$I_{n,m}^\pm(q_z) = \int Z_n^*(z) Z_m(z) e^{\pm iq_z z} dz. \qquad (3.7)$$

Using the approximated expressions of the dielectric tensor components given in Ref. 7, the screening of interband matrix elements is neglected so that

$$|M_{n,m}^{tot}(k,k')|^2 \cong |M_{n,m}^{ext}(k,k')|^2, \qquad (3.8)$$

while intraband screened matrix elements are given for each subband n by
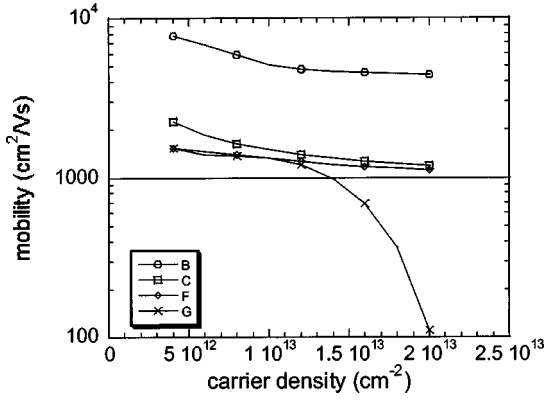
FIG. 4. Theoretical calculation of the mobility at 300 K. Curve G is the mean polynomial representative curve of the experimental points shown Fig. 2. Curve B represents the role of acoustic and optical phonon scattering. Curve C represents the combined effect of phonon and carrier-carrier scattering. Curve F represents the combined effect of phonons, carrier-carrier, impurities ($N_D = 2 \times 10^{18}$ cm^{-3}) or dislocations ($N_{dislo} = 5 \times 10^9$ cm^{-2}) scattering.

$$M_{n,n}^{tot,\pm}(k,k',q_z) = A(\vec{q},q_z)\delta_{k',k\mp q}$$
$$\times \sqrt{\frac{\hbar(N_\kappa + 1/2 \pm 1/2)}{2\rho\omega_\kappa V}} \frac{F_n^\pm(q_z)}{1 + k_{2D}/q},$$
$$(3.9)$$

where

$$F_n^\pm(q_z) = I_{n,n}^\pm(q_z) + \sum_{m \neq n} [I_{n,n}^\pm(q_z) - I_{m,m}^\pm(q_z)] \frac{k_{Sc,m}}{q}.$$
$$(3.10)$$

Their square modulus are given by

$$|M_{n,n}^{tot,\pm}(k,k',q_z)|^2 = \frac{\hbar N_\kappa(1/2 \pm 1/2)}{2\rho\omega_\kappa V} \frac{\delta_{k',k+q}}{(1 + k_{2D}/q)^2}$$
$$\times |A(\vec{q},q_z)F_n^\pm(q_z)|^2. \quad (3.11)$$

Summing over all possible phonon wave vectors, it finally gives

$$|M_{n,n}^{tot,\pm}(k,k')|^2 = \frac{\delta_{k',k\mp q}}{(1 + k_{2D}/q)^2} \frac{\hbar}{4\pi S\rho}$$
$$\times \int_{-\infty}^{\infty} \frac{N_\kappa + 1/2 \pm 1/2}{\omega_\kappa} |A(\vec{q},q_z)F_n^\pm(q_z)|^2 dq_z.$$
$$(3.12)$$

2. Numerical results and discussion

The total effect of acoustic and optical phonon scattering is illustrated Fig. 4, curve B. They lead to mobility values which strongly decrease with increasing carrier density. This strong decrease is a consequence of the progressive spatial localization of the electronic density which allows a larger and larger uncertainty on the electron momentum Oz component and therefore a larger and larger phonon contribution to the 2D electron scattering events. Moreover, increasing the

carrier density also leads to a higher location of the Fermi level, which reaches values (over the first subband ground-state energy) larger than the optical phonon energy as soon as the carrier density reaches $\sim 8 \times 10^{12}$ cm^{-2}. Thus more and more optical phonon emission processes are possible and also contribute to the free-carrier mobility decrease.

Nonetheless, although they naturally lead to a strong decrease of the mobility versus carrier density, phonon scattering mechanisms are far from being able to explain the experimental results represented by the empirical tendency curve shown by the curve G in Fig. 4.

B. Carrier-carrier scattering

For the description of carrier-carrier scattering we have made use of the Episov-Levinson derivation,[21,22] which attributes to each subband a reverse relaxation time given by

$$\frac{1}{\tau_n(k)} = \frac{m^* e^4 n_n}{16\pi(\varepsilon_0\varepsilon_L)^2\hbar^3} \int_0^{2\pi} \frac{F_n^2(q)}{q^2}(1 - \cos\theta)d\theta,$$
$$(3.13)$$

where the form factor $F_n(q)$ is given by

$$F_n(q) = \int e^{-q|z-z'|} |Z_n(z)|^2 |Z_n(z')|^2 dz\, dz'. \quad (3.14)$$

When the carrier-carrier scattering is also taken into account and combined with phonon scattering, it leads to results shown by curve C in Fig. 4. It is noticable to see that when the carrier density reaches values as large as 2×10^{13} cm^{-2}, the mobility values tend approximately towards a constant of the order of 1100 cm^2/V s. In principle, this value should constitute the maximum mobility of the quantum well at large carrier densities.

Obviously, the calculated trend of the carrier mobility and the experimental trend, shown Fig. 2, are clearly different. The sum of phonon and carrier-carrier scattering mechanisms does not explain by itself either the saturation of mobility obtained at low carrier concentration (there is even a decay for $n_s < 4 \times 10^{12}$ cm^{-2}, not shown here, but which will be presented in another work) or the very sharp decay of the mobility that starts at carrier concentrations of 1.4×10^{13} cm^{-2}. Extrinsic mechanisms have therefore to be considered to explain our experimental results.

IV. EXTRINSIC SCATTERING MECHANISMS

A. Impurities and dislocations

Ionized impurities and extended defects like dislocations are standard scattering centers whose associated potentials are well known and will not be recalled in the present paper although, in quantum wells, they also depend on the shape of the wave functions. Concerning dislocations, transmission electron microscope (TEM) observations show that they are mainly made of threading dislocations whose densities are of the order of $\sim 5 \times 10^9$ cm^{-2}. We have thus considered an homogeneous distribution of ionized impurities and of threading dislocations (acting through their possible core charge and through their strain field effects[23]). Introducing

impurity and dislocation scattering in the calculation gives the possibility to decrease and fit the mobility, but only in the range of low carrier densities (the decay, not treated in this paper, for $n_s < 4 \times 10^{12}$ cm^{-2} is mainly due to this kind of defects; it will be treated elsewhere).

Curve F in Fig. 4 shows, for instance, the mobility obtained for a ionized impurity density equal to 2 $\times 10^{18}$ cm^{-3} (so assuming a high background concentration of impurities) and a dislocation density of 5×10^9 cm^{-2}. These results indicate that the low-density regime may be recovered with plausible values of impurities and dislocations. However, due to the increase of the screening effects with increasing carrier densities, impurity and dislocation scattering become negligible compared to intrinsic scattering and can no longer justify the strong mobility decrease observed at large carrier densities.

B. Interface roughness

It is frequently assumed in heterostructures that the interface may not be perfect and bear some interface roughness. Generally, interface roughness effects have been studied in square quantum wells[24–26] where their scattering potential amplitude V_0 is approximately determined by assuming that, locally, the fluctuation of the interface position z of a quantity b (the roughness amplitude) shrinks the well width. Thus, assuming, for instance, an infinitely deep potential of width L, it leads to a modification of the fundamental ground state of the quantum well given by $V_0 = d\varepsilon_1 \cong d(\hbar^2 \pi/2m^*L^2) = -\hbar^2 \pi b/4m^*L^3$. Obviously, this approach is no longer valid in triangular quantum wells (although it was used in Ref. 27) where, in a first approximation, the interface roughness only shifts the potential from a quantity $b: V(z) \rightarrow V(z-b)$. To solve this problem, a direct solution of a 3D Hamiltonian representing an interface with randomly distributed islands was undertaken in Ref. 28. Instead, we have used the following procedure: we may attribute to each point (x,y) a probability $P_b(x,y)$ that the interface is shifted from a distance b. Thus the Hamiltonian of the quantum well in the presence of interface roughness is given by

$$H_{QW} = \frac{p^2}{2m^*} + V(z) + [V(z-b) - V(z)]P_b(x,y)$$

$$= H_{0,QW} + W(x,y,z). \tag{4.1}$$

The $W(x,y,z)$ operator represents the interface roughness scattering potential. As long as this term constitutes a perturbation of the perfect QW Hamiltonian, its matrix elements (entering the definition of the collision time) may be calculated between the eigenstates of the perfect QW Hamiltonian. This gives

$$W_{n,n}(q) = \frac{1}{S} \int e^{-i\vec{k}\cdot\vec{\rho}} |Z_n(z)|^2 W e^{i\vec{k}'\cdot\vec{\rho}} dx\, dy\, dz$$

$$= \frac{1}{S} P_b(q) \int_{-\infty}^{\infty} |Z_n(z)|^2 [V(z+b) - V(z)] dz. \tag{4.2}$$

Since the quantum well potential as well as its wave functions $Z_n(z)$ is known, the integral $V_n = \int |Z_n(z)|^2 [V(z+b) - V(z)] dz$ entering Eq. (4.2) can be determined numerically. The remaining $P_b(q)$ term is the Fourier transform of the "unknown" probability $P_b(x,y)$, which, using a standard result of statistical physics, may always be expressed in the form[29]

$$P_b(q) = S_b \exp\left(\sum_n \frac{(iq)^n}{n!} C_n \right), \tag{4.3}$$

where $C_n = \langle \rho^n \rangle - \langle \rho \rangle^n$ with $\langle \rho^n \rangle = \int \rho^n P_b(\rho) dx\, dy$ and where S_b is a normalizing factor. In the case where the interface roughness is statistically "centrosymmetric," the C_{2n} coefficients only do not vanish so that, if we limit the sum to the second-order term in Eq. (4.3), we obtain[30]

$$P_b(q) = S_b e^{-q^2 d^2/4} \rightarrow P_b(\vec{\rho}) = \frac{S_b}{\pi d^2} e^{-\rho^2/d^2}, \tag{4.4}$$

where we have introduced a correlation length $d = \sqrt{2C_2}$ in order to recover a usual correlation function[8,31] corresponding to the reversed Fourier transform of $P_b(q)$ also shown in Eq. (4.4). The above definition also implies that $S_b = \int P_b(\vec{\rho}) d^2\rho$ represents the area where the interface has been shifted. Introducing Eq. (4.4) into Eq. (4.2), we find

$$W_{n,n}(q) = \frac{S_b}{S} V_n e^{-q^2 d^2/4} = \phi V_n e^{-q^2 d^2/4}, \tag{4.5}$$

where ϕ is a "roughness" coverage ratio.

Opposite to the previous extrinsic scattering centers (ionized impurities and dislocations), the interface roughness scattering mechanisms are efficient together in the low- and large free-carrier density ranges. The right order of magnitude for the low-carrier-density range is found for covering factors ϕ of the order of 0.5 and correlation lengths of the order of $\sim$95 nm [although, obviously, other (ϕ,d) couples of values may be chosen].

Considering, then, phonon, carrier-carrier, and interface roughness mechanisms only, *we could reconstitute the empirical tendency curve describing the experimental trend shown in Fig. 2* (and with curve G in Fig. 4) by arbitrarily choosing $\phi = 0.5$ and by just adjusting the correlation length: this is shown by curve G in Fig. 5. It is worth noting that the whole calculated curve G could be realized introducing quite a regularly decreasing correlation length shown by curve J (scale on the right) in the same figure 5.

V. DISCUSSION AND CONCLUSION

One has just seen that the experimental curve may be exactly reproduced by adjusting the correlation length describing the interface (geometrical) roughness. However, one may question if it is so realistic to consider that the interface roughness could be strongly different from sample to sample: typically here the fitting would show that $Al_xGa_{1-x}N$-GaN interfaces would go rougher as n_S increases, though the epitaxial growth conditions have not changed.

Actually, another meaning can be given to roughness. It is
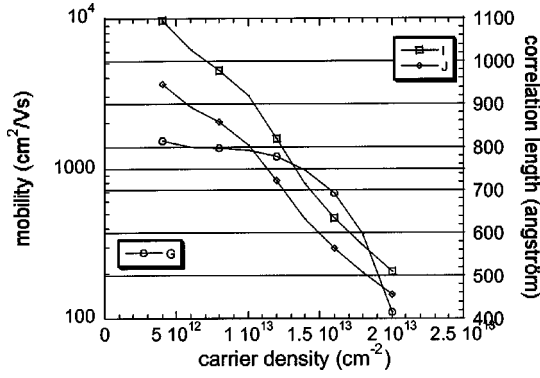
FIG. 5. Curve G gives the exact theoretical fit of the empirical tendency curve (left scale). Curve J (right scale) represents the correlation length needed to describe the interface roughness. Curve I (right scale) represents the correlation length values associated with interface charge spatial fluctuations.

clear that increasing the $Al_xGa_{1-x}N$ thickness as well as the x composition of the alloy, which is needed for obtaining an increasing carrier density n_S, leads to more and more elastic energy stored in the $Al_xGa_{1-x}N$ layer. Thus, as soon as a critical amount of energy is overcome, it is likely that strain relaxation mechanisms start to take place in the heterostructure and progressively destroy the quality of the quantum well itself, although the geometrical interface remains identical. As an example, the atomic force microscopy postgrowth observations of the $Al_xGa_{1-x}N$ surface of samples having a carrier density larger than 1.4×10^{13} cm^{-2} (and therefore a bad mobility) indicates that a network of nanosized V-shaped cracklike defects appears at the $Al_xGa_{1-x}N$ free surface as described in Ref. 32. Since the $Al_xGa_{1-x}N$ layer is under tension, such defects appear in order to release the strain and result most probably into a spatial inhomogeneous strain relaxation. As a consequence, *the piezoelectric interface charge contribution is randomly modified* and depends on the position $\sigma(x,y,z) = \sigma(x,y)\delta(z)$, where $\delta(z)$ is the Dirac function. Other plastical relaxation processes may be imagined as, for instance, some alloy disordering leading to inhomogeneous composition of the alloy and therefore to some spatial inhomogeneous modification of the spontaneous polarization. Also, misfit dislocations may start to be produced contributing here again to inhomogeneous strain relaxation at the interface.

In order to get a general theoretical description of such many mechanisms which finally lead to an inhomogeneous interface charge distribution $\sigma(x,y)$, we propose to approximate the new charge distribution to a binary distribution consisting in regions where the interface charge is not modified and regions appearing with the probability $P(x,y)$ where it is modified by an amount $\langle\delta\sigma\rangle$. Obviously, such a simple description of the inhomogeneous interface charge distribution allows us to make use of the correlation function (4.5) introduced previously. Then, using the Green function technique, the unscreened scattering potential associated with such a charge distribution is given by

$$V(q,z) = \int_{-\infty}^{+\infty} G(q,z,z')\sigma(q,z')dz'$$

$$= \frac{1}{2\varepsilon_0\varepsilon_L q} \int_{-\infty}^{+\infty} e^{-q|z-z'|}\sigma(q,z')dz'$$

$$= \frac{P(q)\langle\delta\sigma\rangle}{2\varepsilon_0\varepsilon_L q} e^{-q|z|}, \tag{5.1}$$

where, for sake of simplicity, we have considered that the two $Al_xGa_{1-x}N$ and GaN media were characterized by the same dielectric constant which allows one to use the standard Green function $G(q,z,z') = \exp(-q|z-z'|)/2\varepsilon_0\varepsilon_L q$. Finally, the unscreened matrix element is given for each subband n by

$$M_{n,n}^{ext}(q) = \int_{-\infty}^{+\infty} |Z_n(z)|^2 V(q,z)dz$$

$$= \frac{\langle\delta\sigma\rangle}{2\varepsilon_0\varepsilon_L q} \phi e^{-q^2 d^2/4} F'(q), \tag{5.2}$$

where the form factor is given by

$$F'(q) = \int_{-\infty}^{+\infty} e^{-q|z|} |Z_n(z)|^2 dz. \tag{5.3}$$

Numerical values corresponding to such potentials have been estimated by choosing arbitrarily $\langle\delta\sigma\rangle \sim \sigma_{pz}$ (the total piezoelectric charge). Curve I in Fig. 5 shows the correlation length versus the carrier density chosen in order to exactly recover the tendency curve. *This last result clearly indicates that the low-mobility regime is consistent with the progressive appearance of relaxation defects which act on the quantum well properties by introducing fluctuations in the interface charge value.*

In conclusion, theoretical investigations of low-field transport in $Al_xGa_{1-x}N$/GaN quantum wells show that one has to expect a natural decrease of the mobility versus the carrier density because of the occurrence of unavoidable scattering mechanisms such as phonons and carrier-carrier interactions which would lead, at high carrier density ($>2 \times 10^{13}$ cm^{-2}) to mobility values of the order of $\sim$1100 cm^2/V s. However, in the actual state of the art, experimental values of the mobility measured on our LP-MOVPE samples are consistent with the appearance of extrinsic scattering mechanisms associated with strain-relaxation-induced defects. They result in a progressive inhomogeneous and random spatial distribution of the interface charge (sort of an interface "electrical roughness") as soon as thick $Al_xGa_{1-x}N$ layers or large x alloy composition values are chosen in order to obtain large carrier densities.

[1] F. Bernardini, V. Fiorentini, and D. Vanderbilt, Phys. Rev. B **56**, R10 024 (1997).

[2] I. P. Smorchkova, C. R. Elsaas, J. P. Ibbetson, R. Vetury, B. Heying, P. T. Fini, E. Haus, S. P. DenBaars, J. S. Speck, and U. K. Mishra, J. Appl. Phys. **86**, 4520 (1999).

[3] J. A. Garrido, J. L. Sanchez-Rojas, A. Jiménez, E. Munoz, F. Omnes, and P. Gibart, Appl. Phys. Lett. **75**, 2407 (1999).

[4] J. P. Ibbetson, P. T. Fini, K. D. Ness, S. P. DenBaars, J. S. Speck, and U. K. Mishra, Appl. Phys. Lett. **77**, 250 (2000).

[5] B. K. Ridley, O. Ambarer, and L. Eastman, Semicond. Sci. Technol. **15**, 270 (2000).

[6] O. Ambacher, J. Majewski, C. Miskys, A. Link, M. Hermann, M. Eickhoff, M. Stutzmann, F. Bernardini, V. Florentini, V. Tilak, B. Schaff, and L. F. Eastman, J. Phys.: Condens. Matter **14**, 3399 (2002).

[7] Jean-Louis Farvacque, Phys. Rev. B **67**, 195324 (2003).

[8] T. Ando, A. B. Fowler, and E. Stern, Rev. Mod. Phys. **54**, 437 (1982).

[9] B. K. Ridley, B. E. Foutz, and L. F. Eastman, Phys. Rev. B **61**, 16 862 (2000).

[10] Z. Bougrioua, J.-L. Farvacque, I. Moerman, and F. Carosella, Phys. Status Solidi B **228**, 625 (2001).

[11] J. Hautman and L. M. Sander, Phys. Rev. B **30**, 7000 (1984).

[12] J. Hautman and L. M. Sander, Phys. Rev. B **32**, 980 (1985).

[13] M. P. Stopa and S. Das Sarma, Phys. Rev. B **47**, 2122 (1993).

[14] D. M. Ceperley and B. J. Alder, Phys. Rev. Lett. **45**, 566 (1980).

[15] J. P. Perdew and A. Zunger, Phys. Rev. B **23**, 5048 (1981).

[16] S. Nagaraja, P. Matagne, V-Y Thean, and J.-P. Leburton, Phys. Rev. B **56**, 15 752 (1997).

[17] D. J. BenDaniel and C. B. Duke, Phys. Rev. **152**, 683 (1966).

[18] D. Brinkmann, Ph.D. thesis, University Grenoble, 1995.

[19] J. L. Farvacque and P. François, Phys. Status Solidi B **223**, 635 (2001).

[20] B. K. Ridley, *Quantum Processes in Semiconductors*, 3rd ed. (Clarendon, Oxford, 1993).

[21] S. E. Episov and I. B. Levinson, Zh. Eksp. Teor. Fiz. **90**, 330 (1986).

[22] B. K. Ridley and N. A. Zakhleniuk, Int. J. High Speed Electron. Syst. **11**, 479 (2001).

[23] J. L. Farvacque, Z. Bougrioua, and I. Moerman, Phys. Rev. B **63**, 115202 (2001).

[24] P. E. Prange and T.-W. Wee, Phys. Rev. **168**, 779 (1968).

[25] T. Ando, J. Phys. Soc. Jpn. **43**, 1616 (1977).

[26] C. Y. Mou and T. M. Hong, Phys. Rev. B **61**, 12 612 (1999).

[27] J. Antoszewski, M. Gracey, J. M. Dell, L. Faraone, T. A. Fisher, G. Parush, Y.-F. Wu, and U. K. Mishra, J. Appl. Phys. **87**, 3900 (2000).

[28] Y. Zhang and J. Singh, J. Appl. Phys. **85**, 587 (1999).

[29] L. E. Reichl, *A Modern Course in Statistical Physics* (Arnold, London, 1998).

[30] Z. Bougrioua, J.-L. Farvacque, and D. Ferré, J. Appl. Phys. **79**, 1536 (1996); **79**, 1546 (1996).

[31] U. Penner, H. Rücker, and I. Yassievich, Semicond. Sci. Technol. **13**, 709 (1998).

[32] Z. Bougrioua, I. Moerman, L. Nistor, B. Van Daele, E. Monroy, E. T. Palacios, F. Calle, and M. Leroux, Phys. Status Solidi A **195**, 93 (2003).